

## AUTHOR QUERY FORM

	<p><b>Journal:</b> Appl. Phys. Lett.</p> <p><b>Article Number:</b> 039717APL</p>	<p>Please provide your responses and any corrections by annotating this PDF and uploading it according to the instructions provided in the proof notification email.</p>
---	--	--

Dear Author,

Below are the queries associated with your article; please answer all of these queries before sending the proof back to AIP. Please indicate the following:

Figures that are to appear as color online only (i.e., Figs. 1, 2, 3) \_\_\_\_\_ (this is a free service).  
 Figures that are to appear as color online and color in print \_\_\_\_\_ (a fee of \$325 per figure will apply).

**Article checklist:** In order to ensure greater accuracy, please check the following and make all necessary corrections before returning your proof.

1. Is the title of your article accurate and spelled correctly?
2. Please check affiliations including spelling, completeness, and correct linking to authors.
3. Did you remember to include acknowledgment of funding, if required, and is it accurate?

Location in article	Query / Remark: click on the Q link to navigate to the appropriate spot in the proof. There, insert your comments as a PDF annotation.
<a href="#">AQ1</a>	Please check that the author names are in the proper order and spelled correctly. Also, please ensure that each author's given and surnames have been correctly identified (given names are highlighted in red and surnames appear in blue).
<a href="#">AQ2</a>	Sections headings are not allowed in APL. Therefore, all headings have been deleted throughout the article.
<a href="#">AQ3</a>	If e-print Refs. 9 and 32 has subsequently been published elsewhere, please provide updated reference information (journal title, volume number, page number, and year).
<a href="#">AQ4</a>	In Ref. 10, please provide a brief description of the information available at the website. For example, "See XX for information about XXX."
<a href="#">AQ5</a>	Refs. 28 and 30 contain identical information. Please check and provide the correct reference or delete the duplicate reference. If the duplicate is deleted, renumber the reference list as needed and update all citations in the text.

Thank you for your assistance.

# 1 Structural and electronic properties of Bi<sub>2</sub>Se<sub>3</sub> topological insulator thin films 2 grown by pulsed laser deposition

AQ1

3 P. Orgiani,<sup>1,2,a)</sup> C. Bigi,<sup>2,3</sup> P. Kumar Das,<sup>2</sup> J. Fujii,<sup>2</sup> R. Ciancio,<sup>2</sup> B. Gobaut,<sup>4</sup> A. Galdi,<sup>1,5</sup>  
4 C. Sacco,<sup>1,6</sup> L. Maritato,<sup>1,6</sup> P. Torelli,<sup>2</sup> G. Panaccione,<sup>2</sup> I. Vobornik,<sup>2</sup> and G. Rossi<sup>2,3</sup>

5 <sup>1</sup>CNR-SPIN, UOS Salerno, 84084 Fisciano, Italy

6 <sup>2</sup>CNR-IOM, TASC Laboratory, 34139 Trieste, Italy

7 <sup>3</sup>Department of Physics, University of Milano, 20133 Milano, Italy

8 <sup>4</sup>Elettra Sincrotrone Trieste, 34139 Trieste, Italy

9 <sup>5</sup>Department of Information and Electrical Engineering and Applied Mathematics, University of Salerno,  
10 84084 Fisciano, Italy

11 <sup>6</sup>Department of Industrial Engineering, University of Salerno, 84084 Fisciano, Italy

12 (Received 20 January 2017; accepted 12 April 2017; published online xx xx xxxx)

13 We report on epitaxial growth of Bi<sub>2</sub>Se<sub>3</sub> topological insulator thin films by Pulsed Laser Deposition  
14 (PLD). X-ray diffraction investigation confirms that Bi<sub>2</sub>Se<sub>3</sub> with a single (001)-orientation can be  
15 obtained on several substrates in a narrow (i.e., 20 °C) range of deposition temperatures and at high  
16 deposition pressure (i.e., 0.1 mbar). However, only films grown on (001)-Al<sub>2</sub>O<sub>3</sub> substrates show an  
17 almost-unique in-plane orientation. *In-situ* spin-resolved angular resolved photoemission spectroscopy  
18 experiments, performed at the NFFA-APE facility of IOM-CNR and Elettra (Trieste), show a  
19 single Dirac cone with the Dirac point at  $E_B \sim 0.38$  eV located in the center of the Brillouin zone  
20 and the spin polarization of the topological surface states. These results demonstrate that the topological  
21 surface state can be obtained in PLD-grown Bi<sub>2</sub>Se<sub>3</sub> thin films. *Published by AIP Publishing.*  
[<http://dx.doi.org/10.1063/1.4982207>]

AQ2

22 Over the last decade, topological insulators have  
23 attracted great interest for their intriguing conduction mech-  
24 anisms.<sup>1-3</sup> Even though they are insulating in the bulk, they  
25 show a metallic surface state characterized by a unique spin  
26 texture, as unambiguously demonstrated by spin-resolved  
27 angular resolved photoemission spectroscopy (ARPES)  
28 experiments.<sup>4-7</sup> Furthermore, these states are topologically  
29 protected against scattering driven by strong spin-orbit  
30 interactions, thus being attractive as functional materials for  
31 spintronic applications.<sup>8,9</sup> However, for both fundamental  
32 studies and electronic applications, high-quality single-  
33 crystalline Bi<sub>2</sub>Se<sub>3</sub> thin films, exhibiting topologically pro-  
34 tected surface states, are therefore necessary. Moreover,  
35 since most of the electronic devices are based on *ad-hoc* tai-  
36 lored multi-layered heterostructures, it is equally necessary  
37 to use flexible thin film deposition techniques which would  
38 allow the growth of a large variety of functional materials  
39 within the same growth system.

40 In a Pulsed Laser Deposition (PLD) system, the single-  
41 atomic species of complex materials are supplied through an  
42 ablation process of a target in the form of polycrystalline  
43 powders and/or single crystal by the irradiation of a high-  
44 intense laser beam. Therefore, multi-layered heterostructures  
45 can be easily engineered by positioning the different targets  
46 along the laser path, in a continuous vacuum condition. PLD  
47 shares with other deposition techniques, such as Molecular  
48 Beam Epitaxy (MBE), the high cleanness of the system to  
49 prevent any possible contamination and the extremely low  
50 deposition rate achievable during the growth (down to  
51 0.01 nm/s). Moreover, since the propagation of the ablated  
52 plume of materials is stopped only at very high pressure (i.e.,

several mbar), deposition processes at such high partial pres- 53  
sures are indeed possible. Such a capability is particularly 54  
important during the growth of materials containing highly 55  
volatile atoms (e.g., selenium in the present case), whose re- 56  
evaporation rate can be reduced by increasing the back- 57  
ground pressure. 58

59 We here report on the growth at very high Ar pressure  
60 (i.e., 0.1 mbar) of Bi<sub>2</sub>Se<sub>3</sub> thin films. Combining low deposi-  
61 tion temperatures ( $\sim 290$  °C) and low deposition rate is the  
62 recipe to epitaxially grow Bi<sub>2</sub>Se<sub>3</sub>. We show that the template  
63 substrate, while not influencing the bulk structural properties,  
64 does have a tremendous impact on the surface structural  
65 properties of the films. Highly textured single domain (001)-  
66 oriented Bi<sub>2</sub>Se<sub>3</sub> can only be grown on (001) Al<sub>2</sub>O<sub>3</sub> substrates.  
67 Our *in-situ* synchrotron radiation x-ray photoemission spec-  
68 troscopy (XPS), angular resolved photoemission spectroscopy  
69 (ARPES) and spin-resolved ARPES data, and *ex-situ*  
70 X-ray diffraction (XRD) data prove that we succeeded in  
71 growing by PLD high quality Bi<sub>2</sub>Se<sub>3</sub> thin films whose surface  
72 hosts the topologically protected surface state with expected  
73 helical spin texture.

74 Bi<sub>2</sub>Se<sub>3</sub> thin films were grown by the PLD technique, at  
75 the NFFA-APE facility of IOM-CNR and Elettra in Trieste,<sup>10</sup>  
76 using a KrF excimer pulsed laser source ( $\lambda = 248$  nm), with a  
77 typical energy density of about 2 J/cm<sup>2</sup>, under a ultra-pure  
78 (99.9999%) Ar pressure. Laser pulses were focused on a stoi-  
79 chiometric polycrystalline Bi<sub>2</sub>Se<sub>3</sub> target (purity 99.999%).  
80 The typical deposition rate was about 0.07 nm per laser shot  
81 and the laser repetition rate was varied from 1 to 10 Hz.  
82 Structural properties of thin films were characterized by *in-*  
83 *situ* Low-Energy Electron Diffraction (LEED) and *ex-situ*  
84 XRD, using a four-circle diffractometer with a Cu K $\alpha$  radi-  
85 ation source. XPS and ARPES measurements were performed

<sup>a)</sup>Electronic mail: pasquale.orgiani@spin.cnr.it

86 at the APE-NFFA beamline end stations receiving undulator  
87 synchrotron radiation from the Elettra storage ring in UHV  
88 spectrometer chambers directly connected with the *in-situ*  
89 PLD growth apparatus, thus allowing the *in-situ* transferring  
90 of the samples.

91  $\text{Bi}_2\text{Se}_3$  shows a rhombohedral crystal structure (space  
92 group R-3m:H) with a periodic stacking of Bi-Se quintuple  
93 layers along the out-of-plane *c*-axis. The unit cell spans three  
94 Bi-Se quintuple layers with lattice constants along the *a*-axis  
95 and *c*-axis of 0.414 nm and 2.864 nm, respectively.<sup>11,12</sup>  
96 Remarkably, even though most of the substrates used for the  
97 growth have very different in-plane lattice parameters (e.g.,  
98 (001)  $\text{Al}_2\text{O}_3$ ,<sup>13</sup> (111)  $\text{SrTiO}_3$ ,<sup>14</sup> (001) Si,<sup>15</sup> (111) Si,<sup>16,17</sup>  
99 and (111) InP<sup>18</sup>), highly *c*-axis oriented  $\text{Bi}_2\text{Se}_3$  thin films  
100 have been deposited in all of the cases. However, azimuthal  
101  $\phi$ -scans typically show a six-fold symmetry rather than the  
102 expected three-fold one, thus indicating that the film in-plane  
103 texturing derives from two domains,  $60^\circ$  rotated with respect  
104 to each other.<sup>13,18,19</sup> We here show that such a two-domain  
105 in-plane texturing can be substantially removed by using a  
106 suitable substrate.

107  $\text{Bi}_2\text{Se}_3$  thin films were deposited on both (001)  $\text{Al}_2\text{O}_3$  and  
108 (111)  $\text{SrTiO}_3$  single crystals. The temperature of the substrate  
109 ranged from  $270^\circ\text{C}$  up to  $400^\circ\text{C}$ . After the film growth, the  
110 samples were cooled down to room temperature in about  
111 30 min in argon at deposition pressure ranging from  $10^{-5}$  up to  
112  $10^{-1}$  mbar. The growth process at low Ar pressure (i.e., below  
113  $10^{-1}$  mbar) was found to promote Bi segregation, as measured  
114 by XPS at the Bi-4f and Se-3d core levels. Similarly, by  
115 increasing the growth temperature, Se deficiency is promoted  
116 until the  $\text{Bi}_3\text{Se}_4$  phase stabilizes for a growth temperature of  
117 about  $330^\circ\text{C}$ . Such a result is not surprising since the  $\text{Bi}_3\text{Se}_4$   
118 shares with the  $\text{Bi}_2\text{Se}_3$  the same rhombohedral crystal struc-  
119 ture, with a slightly larger cell length *a* of 0.422 nm. However,  
120 due to the sizable difference in the *c*-axis lattice parameter  
121 (i.e., 4.04 nm), the two phases can be discriminated by XRD.  
122 A further increase in the temperature turns the film into an  
123 amorphous alloy and no diffraction peaks were measured.  
124 Best results were obtained for a growth temperature of  $290^\circ\text{C}$   
125 and a low repetition rate of laser pulses (i.e., 1 Hz), under an  
126 Ar pressure of  $10^{-1}$  mbar. Interestingly, at such a high deposi-  
127 tion pressure, the target-to-substrate distance was crucial in  
128 getting the optimal Se:Bi chemical ratio. The optimal target-  
129 to-substrate distance, in our geometry, was found to be  
130 48 mm. As a matter of fact, like other complex systems,<sup>20</sup> as  
131 the background pressure increases, the films are deposited  
132 from a progressively more confined ablation plume. This  
133 might selectively affect both the energy and the efficiency of  
134 the single-species transferring to the growing film. This is  
135 what is likely happening also in the case of  $\text{Bi}_2\text{Se}_3$  deposition,  
136 where heavy (i.e., Bi) and light (i.e., Se) elements can be  
137 stopped at different target-to-substrate distances, therefore  
138 determining slight changes in the Bi:Se chemical ratio (e.g.,  
139 samples deposited at a distance of 50 mm are slightly Se  
140 deficient).

141 XRD symmetrical  $\theta$ - $2\theta$  scans of optimized  $\text{Bi}_2\text{Se}_3$  thin  
142 films only contain (00l) peaks, indicating the preferential  
143 *c*-axis orientation of the film along the [001]  $\text{Al}_2\text{O}_3$  and the  
144 [111]  $\text{SrTiO}_3$  substrates' crystallographic directions (Fig. 1).  
145 By symmetric (00 15) Bragg reflections, the out-of-plane

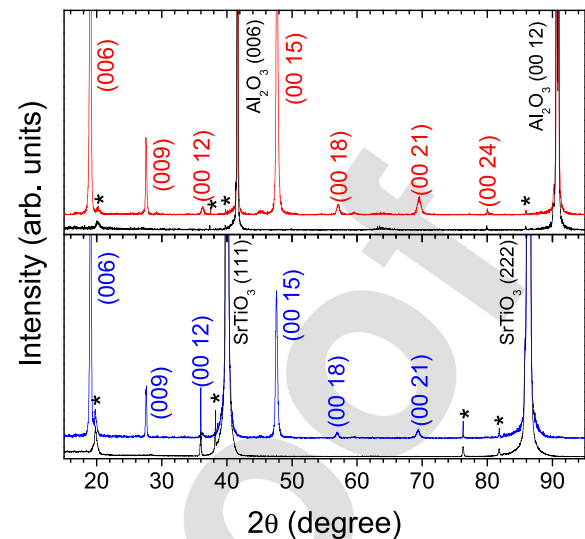


FIG. 1. Symmetrical  $\theta$ - $2\theta$  scan of a  $\text{Bi}_2\text{Se}_3$  thin film grown on a (001)- $\text{Al}_2\text{O}_3$  (red curve in upper panel) and  $\text{SrTiO}_3$  (blue curve in lower panel) substrates. For reference, the spectra of bare (001)- $\text{Al}_2\text{O}_3$  and (111)- $\text{SrTiO}_3$  substrates are also reported as black curves (asterisks indicate spurious peaks recorded using a diffractometer on both films and bare substrates).

*c*-axis parameters were found to be 2.861 nm and 2.862 nm  
for films grown on  $\text{Al}_2\text{O}_3$  and  $\text{SrTiO}_3$  substrates, respec-  
tively, thus indicating a substantial structurally relaxed  
growth on those substrates. The azimuthal  $\phi$ -scan of  $\text{Bi}_2\text{Se}_3$   
thin films grown on  $\text{Al}_2\text{O}_3$  (panel (a) of Fig. 2) shows a sub-  
stantial three-fold symmetry of the film which epitaxially  
grows on C-sapphire with a  $60^\circ$  in-plane rotation of the unit  
cell with respect to the substrate. The very low intensity of  
the second series of diffraction peaks at  $60^\circ$  from the major  
peaks indicates that the double-domain structure is strongly  
suppressed. However, even though showing the same *c*-axis  
preferential orientation,  $\text{Bi}_2\text{Se}_3$  thin films grown on the (111)  
 $\text{SrTiO}_3$  substrate were not well ordered in the surface plane.  
In the azimuthal  $\phi$ -scan (panel (b) of Fig. 2), the second  
series of diffraction peaks is more intense than that reported  
for the film grown on (001)  $\text{Al}_2\text{O}_3$  and the background signal  
is not-zero, thus indicating a fraction of in-plane randomly  
oriented  $\text{Bi}_2\text{Se}_3$  domains.

Since XRD is a bulk sensitive technique, the surface  
order of the PLD grown films was also checked by LEED. In  
full agreement with the bulk sensitive XRD analyses, the  
LEED pattern of *in-situ* transferred  $\text{Bi}_2\text{Se}_3$  thin films grown  
on  $\text{Al}_2\text{O}_3$  (panel (c) of Fig. 2) shows sharp diffraction spots  
exhibiting the expected three-fold symmetry, thus confirm-  
ing the  $\text{Bi}_2\text{Se}_3$  triangular in-plane symmetry. However, films  
grown on the  $\text{SrTiO}_3$  (panel (d) of Fig. 2) show broad dif-  
fraction spots exhibiting a six-fold symmetry with a contin-  
uous connecting ring, indicating the presence of a randomly  
in-plane distributed disordered phase. In the case of  $\text{Bi}_2\text{Se}_3$   
thin films grown on  $\text{SrTiO}_3$  substrates, the surface structural/  
electronic properties can be very unsuitable for device appli-  
cations and/or advanced probing techniques (e.g., spin-  
resolved ARPES experiments on mis-oriented grains lead to  
very broad spectral features or even no detectable band dis-  
persion). On the contrary,  $\text{Bi}_2\text{Se}_3$  thin films grown on (001)  
 $\text{Al}_2\text{O}_3$  show an almost unique in-plane structural arrange-  
ment, thus making them ideal candidates in the cited cases.

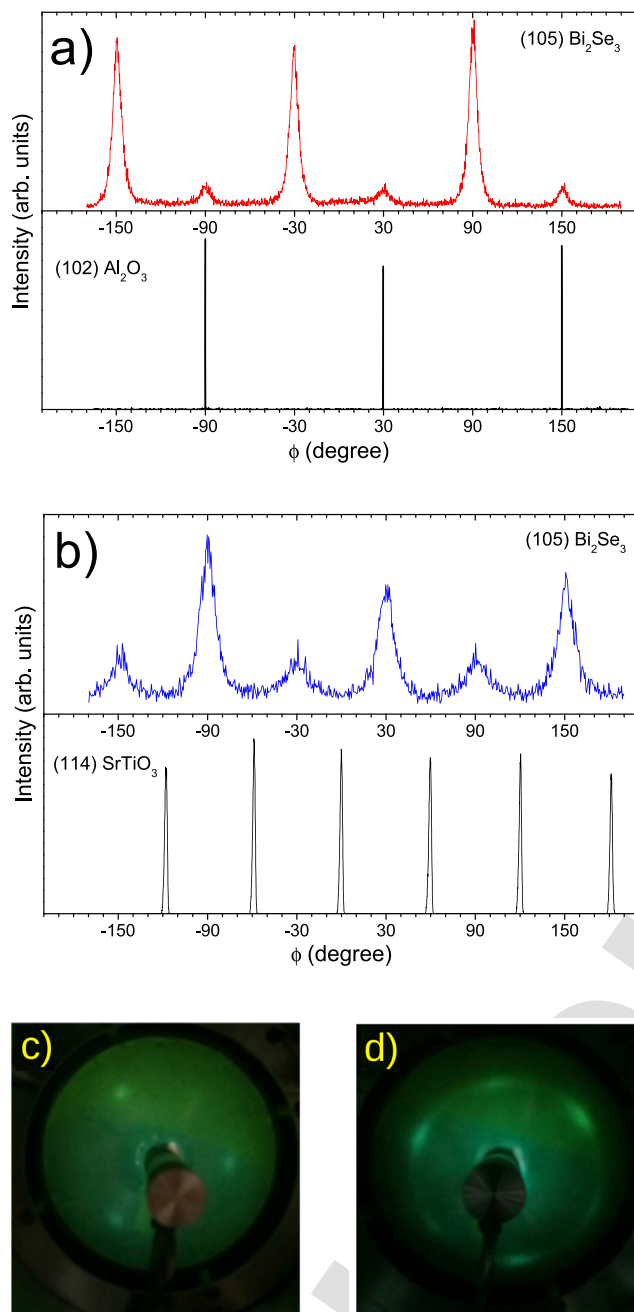


FIG. 2. Azimuthal  $\phi$ -scans around the (105)  $\text{Bi}_2\text{Se}_3$  asymmetric reflections for  $\text{Bi}_2\text{Se}_3$  films grown on  $\text{Al}_2\text{O}_3$  (panel (a)) and  $\text{SrTiO}_3$  (panel (b)) substrates, respectively; as reference, azimuthal  $\phi$ -scans around the (102)  $\text{Al}_2\text{O}_3$  and (114)  $\text{SrTiO}_3$  asymmetric reflections are also reported as black curves in the panels; (c) and (d) LEED patterns of  $\text{Bi}_2\text{Se}_3$  thin films grown on  $\text{Al}_2\text{O}_3$  and  $\text{SrTiO}_3$  substrates, respectively.

183 The electronic properties and the chemical composition  
 184 of  $\text{Bi}_2\text{Se}_3$  thin films were explored by measuring core level  
 185 photoemission spectra. The XPS survey scan displays main  
 186 peaks of both Bi and Se<sup>21–23</sup> with no trace of either Bi<sup>24</sup> or  
 187 Se<sup>25</sup> segregation. In the case of pure Bi clusters, the 4f final  
 188 states would show at 162.3 eV/157.0 eV binding energy  
 189 (panel (a) of Fig. 3); for Se aggregates, the binding would be  
 190 at 55.1/55.3 eV with 0.86 eV spin-orbit splitting, well sepa-  
 191 rated with respect to the observed peaks belonging to  $\text{Bi}_2\text{Se}_3$   
 192 (panel (b) in Fig. 3). Details of the relevant core level peaks  
 193 are presented in the panels of Fig. 3, with the results of fitting  
 194 routines to elucidate the lineshapes and energy separation. In

panel (a), the Bi 4f-Se 3p core lines show Se-related peaks  
 195 shifting by 2.5 eV towards lower binding energies while Bi-  
 196 peaks to higher binding energies (i.e.,  $\Delta E = 0.7$  eV), with  
 197 respect to pure elemental aggregates. Such a behavior, attrib-  
 198 uted to the net charge flow with hybridized bonds between Bi  
 199 and Se, is also observed on other Bi chalcogenide systems.<sup>13</sup>  
 200

Because of the large (i.e., 10%) experimental indetermi-  
 201 nation of the chemical composition from present XPS data  
 202 due to possible errors in the fitting routine and background  
 203 subtraction and the presence of photoelectron diffraction  
 204 effects, as already reported in crystalline topological insula-  
 205 tors,<sup>26,27</sup> we performed energy dispersive spectroscopy  
 206 (EDS) analysis, which is capable of an improved resolution  
 207 in determining the chemical composition (i.e., experimental  
 208 error of about 5%). The Bi:Se chemical ratio was found to be  
 209 1.5, thus indicating a correct stoichiometry of the  $\text{Bi}_2\text{Se}_3$   
 210 thin films. Interestingly, even in the case of a slight Se-deficiency  
 211 (for instance tuned by varying the target-to-substrate distan-  
 212 ce, as previously discussed), the topological properties  
 213 (i.e., a single Dirac cone with well-defined spin-texturing)  
 214 are not lost, while the Dirac cone is rigidly shifted to higher  
 215 binding energies as already reported for thin films<sup>4,6</sup> and also  
 216 for single crystals.<sup>29,30</sup>  
 217

Spin and angular resolved photoemission experiments  
 218 were performed on *in-situ* transferred as-grown  $\text{Bi}_2\text{Se}_3$  thin  
 219 films at a temperature of 77 K and with a synchrotron radia-  
 220 tion spot of about  $100 \times 50 \mu\text{m}$ . In order to better resolve the  
 221 topological surface states features, ARPES investigation was  
 222 performed at a suitable photon energy ( $h\nu = 55$  eV) that  
 223 strongly reduces the photoemission intensity from the bulk  
 224 conduction band. ARPES data of a  $\text{Bi}_2\text{Se}_3$  thin film grown  
 225 on  $\text{Al}_2\text{O}_3$  are shown in Fig. 4.  
 226

The ARPES features (panels (a), (b), and (c) of Fig. 4)  
 227 are in good agreement with the ones measured on cleaved sin-  
 228 gle crystals<sup>28</sup> and thin films grown by MBE.<sup>7</sup> As a matter of  
 229 fact, the characteristic signature of the topological surface  
 230 state can be easily observed: two linearly dispersing metallic  
 231 states cross the Fermi level at  $k_{\parallel} \sim \pm 0.1 \text{ \AA}^{-1}$  and the two  
 232 branches intersecting at  $\Gamma$ . The position of the Dirac point  
 233 was determined by looking at the width of several Momentum  
 234 Distribution Curves (MDCs) of the ARPES spectrum and  
 235 comparing the FWHMs. The Dirac point was estimated to be  
 236 at  $E_B = 0.38 \pm 0.03$  eV binding energy, which is slightly  
 237 larger than the expected value of 300 meV obtained by calcu-  
 238 lations.<sup>3</sup> It is worth noticing that such a discrepancy frequently  
 239 occurs in  $\text{Bi}_2\text{Se}_3$  thin films<sup>13,14</sup> and also in single crystals.<sup>2,7,31</sup>  
 240 Such a result indicates the slight presence of Se vacancies,  
 241 probably near the surface, which act as electron donor sites in  
 242 the  $\text{Bi}_2\text{Se}_3$  compound, populating the conduction band and  
 243 shifting rigidly the band structure towards higher binding  
 244 energies (e.g., for a Se:Bi ratio of about 1.38, the Dirac point  
 245 has been measured at about 0.6 eV). However, charge carrier  
 246 density can be tuned by partially replacing Bi atoms with a  
 247 very small amount ( $\sim 0.6\%$ ) of divalent ions (e.g.,  $\text{Ca}^{2+}$ ), thus  
 248 having the bulk insulating behavior restored.<sup>31</sup>  
 249

The spin texture of the Dirac cone was mapped by using  
 250 a very-low energy electron diffraction (VLEED) based vec-  
 251 torial spin polarimeter recently developed at the APE-NFFA  
 252 beamline.<sup>32</sup> Spin-resolved results, obtained along the quanti-  
 253 zation axis laying in the sample surface plane perpendicular  
 254

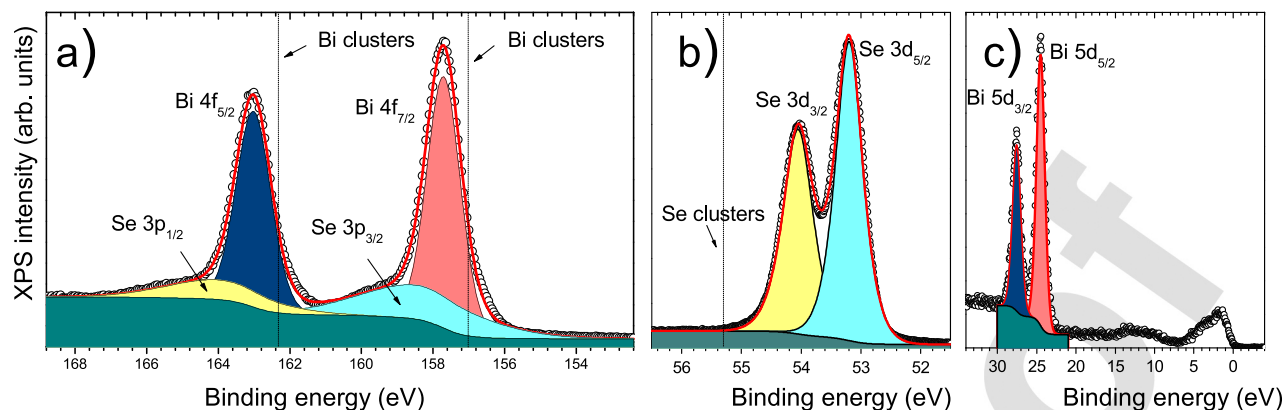


FIG. 3. High-resolution XPS scans of Se-3p/Bi-4f peaks (panel (a)), Se-3d peaks (panel (b)), and Bi-5d peaks along with the valence band (panel (c)); excitation photon energy is 920 eV. Results of fitting procedures are also reported; expected binding energies for both Bi and Se segregation are also reported in panels (a) and (b), respectively.

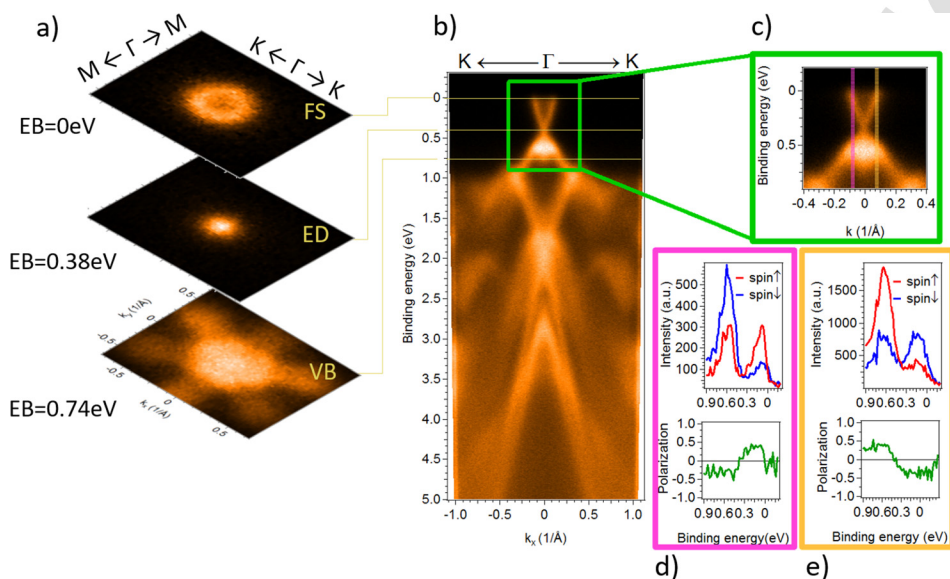


FIG. 4. Spin-ARPES data of the topological surface state of a Bi<sub>2</sub>Se<sub>3</sub> thin film: (a) Constant energy contours at 0 eV ( $E_F$ ), 0.38 eV ( $E_D$ ), and 0.74 eV, respectively; (b) valence band along the K- $\Gamma$ -K high symmetry axis (photon energy is  $h\nu = 55$  eV); (c) zooming out of the topological surface state; (d)–(e) spin-resolved curves and the corresponding spin polarization showing the spin texture of the Dirac cone extracted at  $k_{||} = \pm 0.08 \text{ \AA}^{-1}$ .

255 to the crystalline momentum, are reported in panels (d) and  
 256 (e) of Fig. 4, where the spin-resolved curves and the spin  
 257 polarization deduced from the Energy Distribution Curves  
 258 (EDCs) measured at  $k_{||} = \pm 0.08 \text{ \AA}^{-1}$  in the  $k$ -space are  
 259 shown. In particular, data confirm the expected helical spin  
 260 texture of the topological insulators: namely, two linear  
 261 branches of the Dirac cone spin polarized characterized by  
 262 opposite spin polarization for positive and negative momenta.  
 263 Furthermore, as expected, the spin chirality reverses above  
 264 and below the Dirac point. From the spin polarization analysis,  
 265 the estimated polarization value is  $\sim \pm 40\%$ , lower than  
 266 the expected 100%. However, such a feature is quite common,  
 267 even in the case of single crystals, and it has been discussed  
 268 thoroughly from both the theoretical and experimental  
 269 point of view.<sup>33–35</sup> Nevertheless, from the whole set of both  
 270 ARPES and spin-ARPES results, it can be concluded that the  
 271 PLD-grown Bi<sub>2</sub>Se<sub>3</sub> thin films do show metallic surface states  
 272 that evidence the spin features fingerprints of the topological  
 273 insulators.

274 In conclusion, we have shown that high quality epitaxial  
 275 Bi<sub>2</sub>Se<sub>3</sub> thin films can be grown by Pulsed Laser Deposition.  
 276 The combination of low deposition temperature (i.e., 290 °C),  
 277 high deposition pressure (i.e., 0.1 mbar), and low deposition

rate (i.e., 1 Hz) is crucial to obtain well ordered Bi<sub>2</sub>Se<sub>3</sub> epitax- 278  
 279 ial thin films. Moreover, the use of the (001) Al<sub>2</sub>O<sub>3</sub> substrate  
 280 provides an almost-unique structural texturing of the Bi<sub>2</sub>Se<sub>3</sub>  
 281 thin films. Spin-resolved ARPES data exhibit a single Dirac  
 282 cone with a well-defined spin polarization texture of the topo-  
 283 logical surface states. Moreover, even in the presence of a  
 284 slight Se deficiency, the topological surface states are pro-  
 285 tected and the Dirac cone is rigidly shifted towards higher  
 286 binding energies. Such a feature opens perspectives in emerg-  
 287 ing spintronic planar devices based on multi-layered hetero-  
 288 structures technology in which one functional layer is the  
 289 topological insulator Bi<sub>2</sub>Se<sub>3</sub>. 289

290  
 291 This work has been performed in the framework of the  
 292 Nanoscience Foundry and Fine Analysis (NFFA-MIUR Italy  
 293 Progetti Internazionali) facility. This work has been  
 294 supported by NOXSS PRIN (2012Z3N9R9) Project of  
 295 MIUR, Italy. 295

296  
 297 <sup>1</sup>L. Fu, C. L. Kane, and E. J. Mele, *Phys. Rev. Lett.* **98**, 106803 (2007).  
 298 <sup>2</sup>Y. Xia, D. Qian, D. Hsieh, L. Wray, A. Pal, H. Lin, A. Bansil, D. Grauer,  
 299 Y. S. Hor, R. J. Cava, and M. Z. Hasan, *Nat. Phys.* **5**, 398 (2009).  
 300 <sup>3</sup>H. Zhang, C.-X. Liu, X.-L. Qi, X. Dai, Z. Fang, and S.-C. Zhang, *Nat.*  
 301 *Phys.* **5**, 438 (2009). 301

- 302 <sup>4</sup>S.-Y. Xu, M. Neupane, C. Liu, D. Zhang, A. Richardella, L. A. Wray, N.  
303 Alidoust, M. Leandersson, T. Balasubramanian, J. Sanchez-Barriga, O. Rader,  
304 G. Landolt, B. Slomski, J. H. Dil, J. Osterwalder, T.-R. Chang, H.-T. Jeng, H.  
305 Lin, A. Bansil, N. Samarth, and M. Z. Hasan, *Nat. Phys.* **8**, 616 (2012).  
306 <sup>5</sup>D. Zhang, A. Richardella, D. W. Rench, S.-Y. Xu, A. Kandala, T. C.  
307 Flanagan, H. Beidenkopf, A. L. Yeats, B. B. Buckley, P. V. Klimov, D. D.  
308 Awschalom, A. Yazdani, P. Schiffer, M. Z. Hasan, and N. Samarth, *Phys.*  
309 *Rev. B* **86**, 205127 (2012).  
310 <sup>6</sup>H. M. do Nascimento Vasconcelos, M. Eddrief, Y. Zheng, D. Demaille, S.  
311 Hidki, E. Fonda, A. Novikova, J. Fujii, P. Torelli, B. Rache Salles, I.  
312 Vobornik, G. Panaccione, A. J. Aparecido de Oliveira, M. Marangolo, and  
313 F. Vidal, *ACS Nano* **10**, 1132 (2016).  
314 <sup>7</sup>F. Vidal, M. Eddrief, B. Rache Salles, I. Vobornik, E. Velez-Fort, G.  
315 Panaccione, and M. Marangolo, *Phys. Rev. B* **88**, 241410(R) (2013).  
316 <sup>8</sup>R. Mellnik, J. S. Lee, A. Richardella, J. L. Grab, P. J. Mintun, M. H.  
317 Fischer, A. Vaezi, A. Manchon, E.-A. Kim, N. Samarth, and D. C. Ralph,  
318 *Nature* **511**, 449 (2014).  
319 <sup>9</sup>Y. Kubota, K. Murata, J. Miyawaki, K. Ozawa, M. C. Onbasli, T.  
320 Shirasawa, B. Feng, S. Yamamoto, R.-Y. Liu, S. Yamamoto, S. K.  
321 Mahatha, P. Sheverdyayeva, P. Moras, C. A. Ross, S. Suga, Y. Harada, K.  
322 L. Wang, and I. Matsuda, e-print [arXiv:1604.04869](https://arxiv.org/abs/1604.04869) [cond-mat.mes-hall].  
323 <sup>10</sup>See <http://www.trieste.nffa.eu> ■.  
324 <sup>11</sup>H. Lind, S. Lidin, and U. Hausermann, *Phys. Rev. B* **72**, 184101 (2005).  
325 <sup>12</sup>H. Okamoto, *J. Phase Equilib.* **15**, 195 (1994).  
326 <sup>13</sup>Y. F. Lee, S. Punugupati, F. Wu, Z. Jin, J. Narayan, and J. Schwartz, *Curr.*  
327 *Opin. Solid State Mater. Sci.* **18**, 279 (2014).  
328 <sup>14</sup>P. H. Le, K. H. Wu, C. W. Luo, and J. Leu, *Thin Solid Films* **534**, 659  
329 (2013).  
330 <sup>15</sup>L. Meng, H. Meng, W. Gong, W. Liu, and Z. Zhang, *Thin Solid Films*  
331 **519**, 7627 (2011).  
332 <sup>16</sup>G. Zhang, H. Qin, J. Teng, J. Guo, Q. Guo, X. Dai, Z. Fang, and K. Wu,  
333 *Appl. Phys. Lett.* **95**, 053114 (2009).  
334 <sup>17</sup>P. H. Le, C.-N. Liao, C. W. Luo, J.-Y. Lin, and J. Leu, *Appl. Surf. Sci.*  
335 **285P**, 657 (2013).  
336 <sup>18</sup>S. Schreyeck, N. V. Tarakina, G. Karczewski, C. Schumacher, T.  
337 Borzenko, C. Brüne, H. Buhmann, C. Gould, K. Brunner, and L. W.  
338 Molenkamp, *Appl. Phys. Lett.* **102**, 041914 (2013).  
339 <sup>19</sup>Y. F. Lee, R. Kumar, F. Hunte, J. Narayan, and J. Schwartz, *J. Appl. Phys.*  
340 **118**, 125309 (2015).  
<sup>20</sup>P. Orgiani, R. Ciancio, A. Galdi, S. Amoroso, and L. Maritato, *Appl. Phys.* **341**  
*Lett.* **96**, 032501 (2010). **342**  
<sup>21</sup>J. A. Bearden and A. F. Burr, *Rev. Mod. Phys.* **39**, 125 (1967). **343**  
<sup>22</sup>M. Cardona and L. Ley, *Photoemission in Solids I: General Principles* **344**  
(Springer-Verlag, Berlin, Germany, 1978). **345**  
<sup>23</sup>J. C. Fuggle and N. Mårtensson, *J. Electron Spectrosc. Relat. Phenom.* **21**, **346**  
275 (1980). **347**  
<sup>24</sup>A. S. Hewitt, J. Wang, J. Boltersdorf, P. A. Maggard, and D. B. **348**  
Dougherty, *J. Vac. Sci. Technol. B* **32**, 04E103 (2014). **349**  
<sup>25</sup>Y.-C. Yeh, P.-H. Ho, C.-Y. Wen, G.-J. Shu, R. Sankar, F.-C. Chou, and **350**  
C.-W. Che, *J. Phys. Chem. C* **120**, 3314 (2016). **351**  
<sup>26</sup>K. Kuroda, M. Ye, E. F. Schwier, M. Nurmamat, K. Shirai, M. Nakatake, **352**  
S. Ueda, K. Miyamoto, T. Okuda, H. Namatame, M. Taniguchi, Y. Ueda, **353**  
and A. Kimura, *Phys. Rev. B* **88**, 245308 (2013). **354**  
<sup>27</sup>M. V. Kuznetsov, L. V. Yashina, J. Sanchez-Barriga, I. I. Ogorodnikov, A. **355**  
S. Vorokh, A. A. Volynkov, R. J. Koch, V. S. Neudachina, M. E. Tamm, **356**  
A. P. Sirotnina, A. Y. Varykhalov, G. Springholz, G. Bauer, J. D. Riley, and **357**  
O. Rader, *Phys. Rev. B* **91**, 085402 (2015). **358**  
<sup>28</sup>J. G. Analytis, J.-H. Chu, Y. Chen, F. Corredor, R. D. McDonald, Z. X. **359**  
Shen, and I. R. Fisher, *Phys. Rev. B* **81**, 205407 (2010). **360**  
<sup>29</sup>D. Hsieh, Y. Xia, D. Qian, L. Wray, J. H. Dil, F. Meier, J. Osterwalder, **361**  
L. Patthey, J. G. Checkelsky, N. P. Ong, A. V. Fedorov, H. Lin, A. **362**  
Bansil, D. Grauer, Y. S. Hor, R. J. Cava, and M. Z. Hasan, *Nature* **460**, **363**  
1101 (2009). **364**  
<sup>30</sup>J. G. Analytis, J.-H. Chu, Y. Chen, F. Corredor, R. D. McDonald, Z. X. **365**  
Shen, and I. R. Fisher, *Phys. Rev. B* **81**, 205407 (2010). **366**  
<sup>31</sup>Z. Wang, T. Lin, P. Wei, X. Liu, R. Dumas, K. Liu, and J. Shi, *Appl. Phys.* **367**  
*Lett.* **97**, 042112 (2010). **368**  
<sup>32</sup>C. Bigi, J. Fujii, I. Vobornik, P. K. Das, D. Benedetti, F. Salvador, G. **369**  
Panaccione, and G. Rossi, e-print [arXiv:1610.06922](https://arxiv.org/abs/1610.06922) [physics.ins-det]. **370**  
<sup>33</sup>O. V. Yazyev, J. E. Moore, and S. G. Louie, *Phys. Rev. Lett.* **105**, 266806 **371**  
(2010). **372**  
<sup>34</sup>Z.-H. Zhu, C. N. Veenstra, S. Zhdanovich, M. P. Schneider, T. Okuda, K. **373**  
Miyamoto, S.-Y. Zhu, H. Namatame, M. Taniguchi, M. W. Haverkort, I. **374**  
S. Elfimov, and A. Damascelli, *Phys. Rev. Lett.* **112**, 076802 (2014). **375**  
<sup>35</sup>G. Landolt, S. Schreyeck, S. V. Ereemeev, B. Slomski, S. Muff, J. **376**  
Osterwalder, E. V. Chulkov, C. Gould, G. Karczewski, K. Brunner, H. **377**  
Buhmann, L. W. Molenkamp, and J. H. Dil, *Phys. Rev. Lett.* **112**, 057601 **378**  
(2014). **379**

AQ5

AQ3  
AQ4